[Regular Paper]

Effects of Ruthenium Precursors on $Ru/Mn/Al_2O_3$ and Ru/Al_2O_3 Catalysts for Fischer-Tropsch Synthesis

Mohammad NURUNNABI*, Kazuhisa MURATA, Kiyomi OKABE, Toshiaki HANAOKA, Tomohisa MIYAZAWA, and Kinya SAKANISHI

Biomass Technology Research Center, National Institute of Advanced Industrial Science and Technology, AIST Chugoku, Suehiro 2-2-2, Hiro, Kure, Hiroshima 737-0197, JAPAN

(Received August 20, 2009)

$Ru/Mn/Al_2O_3$ and Ru/Al_2O_3 catalysts, which prepared with various ruthenium precursors into impregnation method, were investigated for Fischer-Tropsch (FT) synthesis in a continuous stirred tank reactor; and the catalysts were characterized by H_2-chemisorption, TPR, XRD, TEM and XPS. On the basis of $Ru/Mn/Al_2O_3$ catalysts, $Ru(Cl)/Mn/Al_2O_3$ prepared with ruthenium chloride exhibited much higher catalytic activity and stability than those on $Ru(A)/Mn/Al_2O_3$ and $Ru(N)/Mn/Al_2O_3$, which were prepared with ruthenium acetylacetonate and ruthenium nitrosyl nitrate precursors. The order of the CO conversion was $Ru(Cl)/Mn/Al_2O_3 \gg Ru(A)/Mn/Al_2O_3 > Ru(N)/Mn/Al_2O_3$. This order was also agreed with the order of CO conversion on Ru/Al_2O_3 in various ruthenium precursors. One explanation is in characterization results that the particle size of Ru and the pore diameter of the support such as 8 nm can be performed to influence high FT activity. On the other hand, over $Ru(Cl)/Mn/Al_2O_3$ and $Ru(Cl)/Al_2O_3$ catalysts, lower activity and higher deactivation rate with reaction time on $Ru(Cl)/Al_2O_3$ were clearly observed, where $Ru(Cl)/Mn/Al_2O_3$ showed high resistance to catalyst deactivation. In this observation, manganese chloride can be formed by removing chlorine atoms from ruthenium chloride, thus increasing the concentration of metallic Ru active species on the catalyst surface and with inhibiting catalyst deactivation.

Keywords

Ruthenium precursor, Ruthenium catalyst, Fischer-Tropsch synthesis, Catalyst activity, Deactivation rate

1. Introduction

As an industrial interested in the area of alternative energy, the diesel fuels can be produced by a suitable Fischer-Tropsch (FT) catalyst from the natural resources such as biomass, coal or natural gas into BTL (biomass to liquid) and GTL (gas to liquid) technologies[1)~6)]. The diesel is a very high-performance alternative clean fuel and it can enable reduction in emission of greenhouse gases for solving energy and global environmental problems. It has a very high cetane number and very low sulphur, particulate matter and aromatic contents. A metal such as Ru may provide to prepare a suitable FT catalyst for the production of diesel fuels. On the basis of higher catalytic activity, selectivity and stability[7)~11)], Ru metal is the most active for FT synthesis in a continuous stirred tank reactor at low reaction temperature. However, Ru metal has problems in the cost and limited availability. In the Ru precursors, ruthenium chloride is available in the market and cheaper than other Ru precursors. In the catalyst preparation from ruthenium chloride as a precursor, chlorine can present on the catalyst surface. It is well known that chlorine is a poison for CO and H_2 chemisorptions and it can be partitioned between the support and the metal[12),13)]. Therefore, new catalysts with high activity and stability are needed for FT synthesis. Mn addition can promote FT activity and stability by using a suitable support in the catalysts[14),15)]. Previous reports suggested that a γ-Al_2O_3 support is more effective in presence of Mn for FT synthesis[16)~18)]. In this article, we report the effects of Ru precursors on catalytic performance for a $Ru/Mn/Al_2O_3$ catalyst in a slurry phase FT reaction. Moreover, catalyst characterization results were investigated according to the H_2-chemisorption, BET surface area, BJH porosity, XRD, TPR, TEM and XPS measurements.

2. Experimental

2. 1. Catalyst Preparation

$Ru/Mn/Al_2O_3$ and Ru/Al_2O_3 catalysts were prepared by the impregnation method using γ-Al_2O_3 support (Soekawa Chemical Co., Ltd., Japan; 2-3 μm). At first the support was impregnated with an aqueous solution

* To whom correspondence should be addressed.
* E-mail: mohammad-nabi@aist.go.jp

Table 1 BET Surface Area, BJH Porosity, H_2 Chemisorption, XRD and TEM Results on $Ru/Mn/Al_2O_3$ Catalysts

Catalyst	BET [m^2/g]	Pore volume [cm^3/g]	Pore diameter [nm]	H_2 adsorption [cm^3/g STP]	Dispersion of Ru [%]	Particle size [nm]		
						XRD	H_2ad	TEM
$Ru(Cl)/Mn/Al_2O_3$	69	0.17	8.4	1.22	22.0	8.1	7.3	7.9
$Ru(A)/Mn/Al_2O_3$	75	0.18	8.9	0.76	13.7	9.9	11.6	9.6
$Ru(N)/Mn/Al_2O_3$	72	0.18	8.8	1.37	24.7	6.1	6.5	6.3
$Ru(Cl)/Al_2O_3$	81	0.19	8.2	—	—	8.4	—	8.3
$Ru(A)/Al_2O_3$	80	0.18	8.7	—	—	14.1	—	—
$Ru(N)/Al_2O_3$	81	0.19	8.5	—	—	12.6	—	—

of $Mn(NO_3)_2 \cdot 6H_2O$ (Wako Pure Chemical Industries Ltd., Japan) and then removed the solvent by evaporation at 348 K. After drying at 383 K overnight, the sample (Mn/Al_2O_3) was calcined in air at 873 K for 5 h. In this study, Mn to Al molar ratio was 1/4. In the next step, the sample was impregnated with an aqueous solution of $RuCl_3 \cdot nH_2O$ (Soekawa Chemical, Japan) or $Ru(NO_3)_3(NO)$ (Soekawa Chemical, Japan) or an acetone solution of $Ru(C_5H_7O_2)_3$ (Soekawa Chemical, Japan). After removal of the solvent by heating, the catalysts were dried in an oven overnight at 383 K. Subsequently, the catalysts were calcined in air at 673 K for 4 h. The loading amount of Ru used was 5 wt%. The prepared catalysts are denoted as $Ru(Cl)/Mn/Al_2O_3$, $Ru(N)/Mn/Al_2O_3$ and $Ru(A)/Mn/Al_2O_3$ or $Ru(Cl)/Al_2O_3$, $Ru(N)/Al_2O_3$ and $Ru(A)/Al_2O_3$ according to the solution of $RuCl_3 \cdot nH_2O$, $Ru(NO_3)_3(NO)$ and $Ru(C_5H_7O_2)_3$, respectively. BET surface area of these catalysts (from nitrogen porosimetry) is listed in **Table 1**.

2. 2. Catalyst Characterization

X-ray diffraction (XRD) was measured after catalyst calcination and H_2 reduction by using a Mac Science M18XHF22-SRA diffractometer with Cu Kα radiation at 40 kV and 150 mA.

The BET surface area and BJH pore size distribution of the catalysts were estimated by using a Belsorp-max instrument with adsorption-desorption isotherm of N_2 at 77 K.

The amount of hydrogen chemisorption of the catalysts was determined by using an auto-apparatus ASAP-2000 at 308 K.

The reducibility of the catalysts was characterized by a temperature-programmed reduction with H_2 (H_2-TPR) technique. Before the TPR measurement, the samples (about 22.0 mg) were heated at 773 K for 20 min (heating rate 10 K/min) under Ar gas flow of 30 m*l*/min in order to remove any adsorbed species such as CO_2. After the sample was cooled down to room temperature under Ar flowing, the reactor was heated again from room temperature to 870 K at a heating rate of 10 K/min and then the temperature was maintained for 0.5 h in a 5% H_2/Ar mixture gas flow of 35 m*l*/min. The temperature was measured by using a thermocouple located in the catalyst bed. The H_2 consumption was continuously monitored by thermal conductivity detector-gas chromatography (TCD-GC).

The catalyst sample, reduced by H_2 at 473 K for 5 h under 20 bar (1 bar = 1×10^5 Pa), was analyzed using FEI Tecnai G2 F20 transmission electron microscope (TEM) operating at 200 keV. The powdered catalyst sample was distributed on a carbon film mounted over copper grid, and rested on a sample holder. TEM images were collected through energy filter, which eliminates electrons inelastically scattered. The sample was first observed in the energy filtered TEM. When the sample attracted our interest, we switched to scanning transmission electron microscopy (STEM) mode, in which probe was converged (<1 nm) and high-angle annular dark field (HAADF) detector was inserted into beam path. Energy dispersive X-ray spectroscopy (EDS) was also employed to identify the sample composition in both TEM and STEM modes. In the energy filtered TEM mode, EDS spectra give us information of bulk composition, while in the STEM mode, area exposed is very limited, bringing us local compositional information.

X-ray photoelectron spectroscopy (XPS) measurements were analyzed by using a Shimadzu ESCA-850 with Mg-K$_\alpha$ irradiation (8 kV, 30 mA). XPS data of the samples were collected with H_2 reduction pretreatment after evacuation conditions at 473 K and 10^{-9} bar for 3 h within the pre-chamber, which connected to the vacuum system of the apparatus. The binding energies of XPS were referred to contamination C on the surface of the sample as the internal standard with C_{1s} level at 284.6 eV.

2. 3. Catalytic Reaction

FT synthesis was carried out in a 0.3 *l* autoclave slurry continuous stirred tank reactor (CSTR). The illustration of this reactor was reported previously[16]. The catalyst was reduced with hydrogen at 473 K, 20 bar for 5 h in this reactor. After hydrogen reduction, the catalyst was suspended by using 80 g hexadecane as a solvent under atmospheric pressure and room temperature. The amount of catalyst used was 2.5 g and the partial pressure ratio of reactants was $H_2/CO/Ar = 6/3/1$. The reactions were carried out at $T = 493$ K, $P = 20$ bar, GHSV = 1800 h^{-1}. The feed gas flow rate was adjusted with a mass flow controller and the reaction temperature was monitored by the inside and outside thermocouples

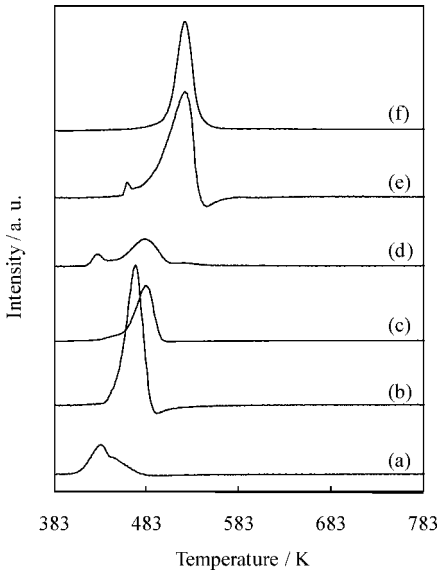

Fig. 1 TPR Profiles of (a) $Ru(A)/Al_2O_3$, (b) $Ru(N)/Al_2O_3$, (c) $Ru(Cl)/Al_2O_3$, (d) $Ru(A)/Mn/Al_2O_3$, (e) $Ru(N)/Mn/Al_2O_3$ and (f) $Ru(Cl)/Mn/Al_2O_3$ Catalysts at 300-800 K

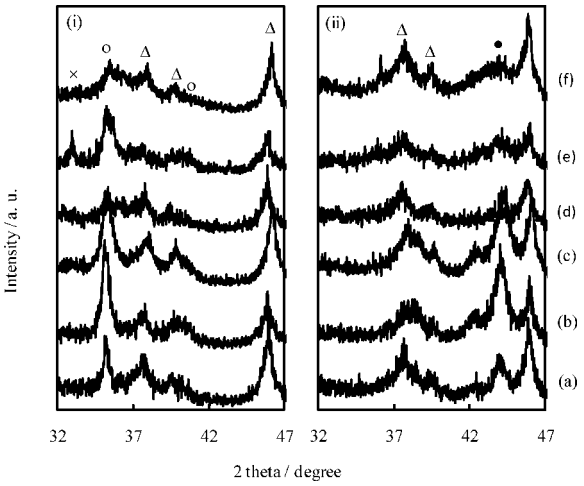

(×) Mn_2O_3, (○) RuO_2, (△) γ-Al_2O_3, (●) Ru^0.

Fig. 2 XRD Patterns of (a) $Ru(A)/Al_2O_3$, (b) $Ru(N)/Al_2O_3$, (c) $Ru(Cl)/Al_2O_3$, (d) $Ru(A)/Mn/Al_2O_3$, (e) $Ru(N)/Mn/Al_2O_3$ and (f) $Ru(Cl)/Mn/Al_2O_3$ Catalysts after (i) Calcination and (ii) H_2 Reduction

of autoclave. The product gas was periodically analyzed with Shimadzu on-line gas chromatographs (GC-2014) in both hydrogen-flame ionization detector (FID) and TCD, and the liquid hydrocarbons were analyzed after reaction by another Shimadzu gas chromatograph (GC-8A). Experimental details were described in a previous report[16].

3. Results and Discussion

TPR profiles of $Ru/Mn/Al_2O_3$ and Ru/Al_2O_3 catalysts in the temperature ranges of 300-800 K are shown in **Fig. 1**. In the catalyst preparation from various ruthenium precursors by the impregnation method, the solution of ruthenium chloride, ruthenium acetylacetonate and ruthenium nitrosyl nitrate were used to prepare Ru catalysts, which denoted as $Ru(Cl)/Mn/Al_2O_3$, $Ru(A)/Mn/Al_2O_3$ and $Ru(N)/Mn/Al_2O_3$ or $Ru(Cl)/Al_2O_3$, $Ru(A)/Al_2O_3$ and $Ru(N)/Al_2O_3$, respectively. Over $Ru/Mn/Al_2O_3$ catalysts, two hydrogen consumption peaks were observed in both $Ru(A)/Mn/Al_2O_3$ and $Ru(N)/Mn/Al_2O_3$, **Figs. 1(d)** and **(e)**. In $Ru(A)/Mn/Al_2O_3$ there was a small shoulder peak centered near 430 K representing the possible reduction of incompletely decomposed $Ru(C_5H_7O_2)_3$. There was a main broader hydrogen reduction peak near 480 K corresponding to the reduction of RuO_2 to Ru^0 [19)~22)]. $Ru(N)/Mn/Al_2O_3$ showed a quite similar reduction peaks with $Ru(A)/Mn/Al_2O_3$, and centered near 463 and 525 K. The lower temperature smaller peak can also be represented to the reduction of incompletely decomposed $Ru(NO_3)_3(NO)$. In contrast, the high temperature broader peak intensity, which was attributed to the reduction of RuO_2, was much higher on $Ru(N)/Mn/Al_2O_3$ than that on $Ru(A)/Mn/Al_2O_3$. On the other hand, in **Fig. 1(f)**, $Ru(Cl)/Mn/Al_2O_3$ showed only one hydrogen reduction peak at 525 K assigned to the reduction of RuO_2 to Ru^0. There was no another peaks assigned to the ruthenium chloride or ruthenium oxychloride in $Ru(Cl)/Mn/Al_2O_3$. Ruthenium chloride can be oxidized into RuO_2 at the catalyst surface after calcined in air. This result is also consistent with previous reports[20),21)]. The formation of RuO_2 at the catalyst surface was also confirmed by the XRD diagram. In the case of Ru/Al_2O_3 catalysts, $Ru(A)/Al_2O_3$ showed two peaks assigned to the reduction of RuO_2 to RuO to Ru^0 in two steps (**Fig. 1(a)**). However in **Figs. 1(b)** and **(c)**, $Ru(N)/Al_2O_3$ and $Ru(Cl)/Al_2O_3$ exhibited one hydrogen reduction peak assigned to the reduction of RuO_2 to Ru^0. For comparison, $Ru/Mn/Al_2O_3$ showed a delay reduction peak with respect Ru/Al_2O_3, and reduction peaks attributed to the Mn-species interaction forcing the RuO_2 phase to be reduced at a higher temperature. Catalyst characterization results are also listed in **Table 1**. The difference of the amount of hydrogen adsorption was observed over $Ru/Mn/Al_2O_3$ catalysts, and $Ru(A)/Mn/Al_2O_3$ showed low hydrogen adsorption and low metal dispersion than $Ru(Cl)/Mn/Al_2O_3$ and $Ru(N)/Mn/Al_2O_3$ catalysts. In BET surface area, there was almost similar result over the catalysts. This means low reducibility of $Ru(A)/Mn/Al_2O_3$ due to a possible strong Ru–Mn–Al species interaction forcing the RuO_2 phase to be hardly reduced on the catalyst surface.

Figure 2 shows the XRD diffractograms of $Ru(Cl)/Mn/Al_2O_3$, $Ru(A)/Mn/Al_2O_3$, $Ru(N)/Mn/Al_2O_3$, $Ru(Cl)/Al_2O_3$, $Ru(A)/Al_2O_3$ and $Ru(N)/Al_2O_3$ catalysts. After

catalyst calcination in air (**Fig. 2(i)**), the peaks assigned to the formation of RuO_2[23] were clearly observed in $Ru/Mn/Al_2O_3$ and Ru/Al_2O_3 catalysts prepared with various Ru precursors. In an observation by XRD patterns with reduced catalysts (**Fig. 2(ii)**), the peaks of Ru metal[24] were formed due to complete reduction of RuO_2 over the catalysts. The main diffraction peak of Ru was presented at $2\theta = 44°$. The crystallite size of Ru was measured using the Scherrer equation after catalyst reduction, and these results are shown in **Table 1**. It is clear that $Ru(Cl)/Mn/Al_2O_3$ and $Ru(Cl)/Al_2O_3$ showed middle size Ru crystallites such as 8 nm than the sizes of $Ru(A)/Mn/Al_2O_3$, $Ru(N)/Mn/Al_2O_3$, $Ru(A)/Al_2O_3$ and $Ru(N)/Al_2O_3$ catalysts. These agreed with those obtained from the results of H_2 adsorption (**Table 1**). Another point is the formation of Mn-species in $Ru/Mn/Al_2O_3$ catalysts. In **Fig. 2(i)**, the peak assigned to Mn_2O_3[25] were clearly observed over $Ru(N)/Mn/Al_2O_3$ sample; and $Ru(A)/Mn/Al_2O_3$ yield a very low intensity diffraction peak of Mn_2O_3 than that on $Ru(N)/Mn/Al_2O_3$. Other Mn-species such as $MnCl_2$ in $Ru(Cl)/Mn/Al_2O_3$ was not observed on the catalyst surface, possibly this species is below the limit of detection by XRD.

Figure 3 represents the TEM images of $Ru/Mn/Al_2O_3$ catalysts after H_2 reduction at 473 K, where uniformly dispersed particles were observed. According to the zero-loss TEM images in **Figs. 3(a)-3(c)**, we observed a lot of round-shaped particles, which corresponds to Ru metals over $Ru(Cl)/Mn/Al_2O_3$ catalyst (**Fig. 3(c)**), where no such ruthenium particles were observed over $Ru(A)/Mn/Al_2O_3$ and $Ru(N)/Mn/Al_2O_3$ catalysts (**Figs. 3(a)** and **3(b)**). However, it is possible to measure the average particle size (d) of Ru by using the equation of $d = \sum_i n_i d_i^3 / \sum_i n_i d_i^2$ (n_i: number of the particles; d_i: particle size) and it is listed in **Table 1**. This also agreed with those from XRD and H_2 adsorption (**Table 1**).

Figure 3(d) shows the HAADF-STEM image over $Ru(Cl)/Mn/Al_2O_3$ catalyst. In the dark field image, we observed brighter spots with round-shaped, which indicate to compose of Ru particles by comparing to the zero-loss image **(Fig. 3(c))**. An EDS spectrum, which is shown in **Fig. 3(e)**, was obtained for $Ru(Cl)/Mn/Al_2O_3$ catalyst at a spot indicated in **Fig. 3(d)**. The elements of Ru, Mn, Al, O and Cl were clearly observed over $Ru(Cl)/Mn/Al_2O_3$ catalyst. This finding gives clear evidence for the presence of Mn and Cl elements on the surface of $Ru(Cl)/Mn/Al_2O_3$, and it was also measured in the XPS data.

Table 2 shows the surface atomic concentrations and binding energies of $Ru(Cl)/Mn/Al_2O_3$ and $Ru(Cl)/Al_2O_3$ catalysts after H_2 reduction at 473 K and 10^{-9} bar inside the XPS pre-chamber. It is seen that atomic concentrations of Ru and Cl were pretty different in both

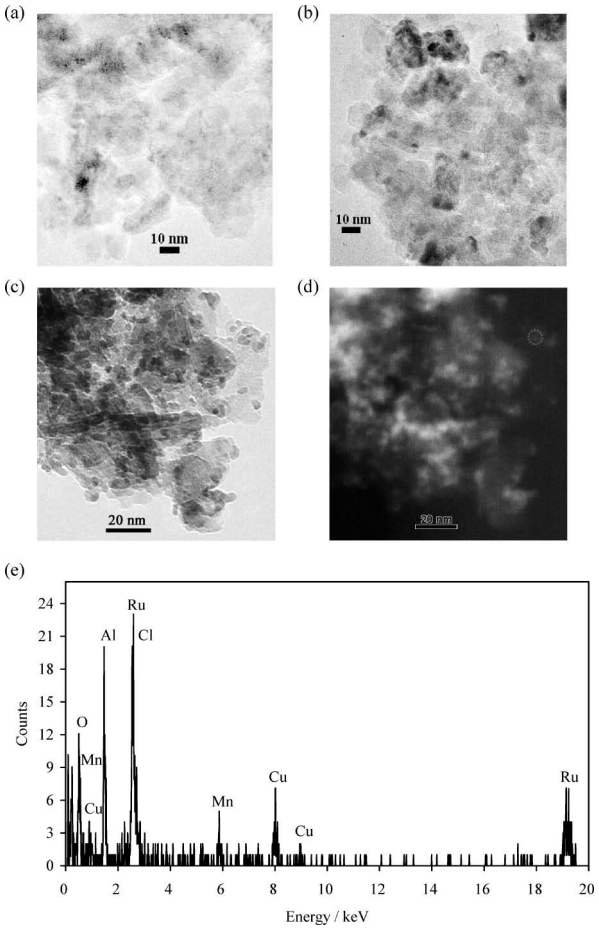

(a, b, c) zero-loss TEM, (d) HAADF-STEM and (e) EDS spectra.

Fig. 3 TEM Images of (a) $Ru(A)/Mn/Al_2O_3$, (b) $Ru(N)/Mn/Al_2O_3$ and (c, d) $Ru(Cl)/Mn/Al_2O_3$ Catalysts after H_2 Reduction at 473 K

catalysts, and the concentration of Ru was higher on $Ru(Cl)/Mn/Al_2O_3$ than that on $Ru(Cl)/Al_2O_3$. On the other hand, $Ru(Cl)/Mn/Al_2O_3$ and $Ru(Cl)/Al_2O_3$ showed almost similar pore diameter and particle size of ruthenium in **Table 1**. These suggest that higher surface concentration of ruthenium was not related with the size of ruthenium particles and pore diameters, and the catalyst reducibility can be improved by the formation of Mn-species. The ratio of Al/O in the concentration of Al and O was observed for the formation condition of Al_2O_3. The atomic concentration of Mn on the surface of $Ru(Cl)/Mn/Al_2O_3$ was observed after catalyst reduction, and the value of Cl/Mn ratio was about 0.9. This value was lower than 2 for the condition of $MnCl_2$ formation on the catalyst surface, and we focused this ratio on the formation of $MnCl_2$ in our previous report[26]. Therefore, the binding energy values of Mn 2p were also observed in **Fig. 4** and in **Table 2**. In **Table 2**, the energy values of Mn 2p over $Ru(Cl)/Mn/Al_2O_3$ was 642.2 eV. This value can indicate that Mn can remain in the oxidic or chloride species according to the previ-

ous reports[14),27)]. In **Fig. 4**, the peak shapes and binding energy positions of Mn 2p were observed over Mn_2O_3, $MnCl_2$ and Ru(Cl)/Mn/Al_2O_3. It is clear that Mn_2O_3 showed one energy peak at 640.9 eV (**Fig. 4(a)**), and $MnCl_2$ showed two energy peaks at 641.9 eV assigned to the $MnCl_2$ and at 641.0 eV assigned to the Mn-oxide (**Fig. 4(b)**). These values are also in agreement with a previous report[27)]. On the other hand, in **Fig. 4(c)**, Ru(Cl)/Mn/Al_2O_3 showed one binding energy peak at 642.2 eV and this value was compared with the values of bulk compound of $MnCl_2$ and Mn_2O_3. It is seen that the energy position of Ru(Cl)/Mn/Al_2O_3 was almost similar with the value of $MnCl_2$ at 641.9 eV. It can be suggested that Mn can accelerate a removal of Cl atom from $RuCl_3$, and it can be closely related to the formation of $MnCl_2$ on the catalyst surface in Ru(Cl)/Mn/Al_2O_3 prepared with ruthenium chloride precursor. Furthermore, the binding energy values of Ru 3p were observed in **Table 2**. The energy values of Ru 3p were 461.7 and 461.3 eV over Ru(Cl)/Mn/Al_2O_3 and Ru(Cl)/Al_2O_3, respectively. This suggests the reduction of RuO_2 to Ru^0 on the catalyst surface[20),22)]. In addition, the binding energy values of Ru 3p were also observed at 465 eV over Ru(Cl)/Al_2O_3. This value can be assigned to the ruthenium oxychlorides ($RuCl_xO_y$), which can strongly interact with the surface of support, and it can lead to decrease the concentration of metallic Ru active species on the catalyst surface. It is also supported by the previous report[22)]. However, this mechanism will be reported in the future study.

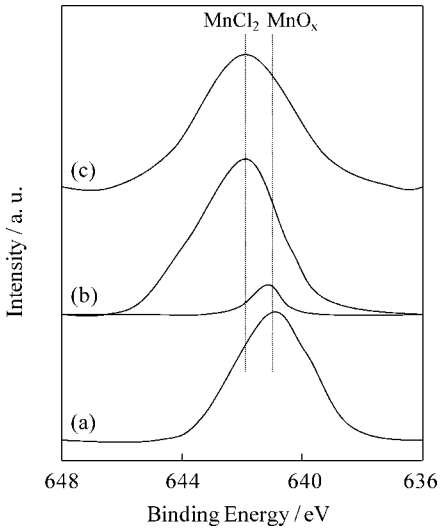

Evacuation treatment at 473 K and 10^{-9} bar for 3 h inside the XPS pre-chamber.

Fig. 4 Mn $2p_{3/2}$ XPS Spectra of (a) Mn_2O_3, (b) $MnCl_2$ and (c) Ru/Mn/Al_2O_3

Figure 5 shows the reaction time dependence on CO conversion and deactivation rate over Ru(Cl)/Mn/Al_2O_3, Ru(A)/Mn/Al_2O_3, Ru(N)/Mn/Al_2O_3, Ru(Cl)/Al_2O_3, Ru(A)/Al_2O_3 and Ru(N)/Al_2O_3 catalysts for FT synthesis at 493 K, 20 bar and 1800 h^{-1}. On the basis of Ru/Mn/Al_2O_3 catalysts with various ruthenium precursors, Ru(N)/Mn/Al_2O_3 showed much low CO conversion during the reaction, **Fig. 5(a)**. This conversion was lower than 20%. In contrast, Ru(A)/Mn/Al_2O_3 exhibited higher CO conversion than that on Ru(N)/Mn/Al_2O_3, and CO conversion was about 77% at the initial stage of reaction. However, CO conversion decreased significantly with time on stream in both catalysts, and this profile corresponds to the catalyst deactivation rate. The deactivation rate was clearly observed in **Fig. 5(b)** and this rate increased with increasing the reaction time over the catalysts. On the other hand, Ru(Cl)/Mn/Al_2O_3, which prepared with ruthenium chloride, enhanced the CO conversion remarkably and the deactivation rate was negligible with time on stream. In Ru(Cl)/Mn/Al_2O_3, the amount of CO conversion was estimated to be about 80% at 40 h time on stream. In the case of Ru/Al_2O_3, it is clear that CO conversion over Ru(Cl)/Al_2O_3 was much higher than that on Ru(N)/Al_2O_3 and Ru(A)/Al_2O_3 catalysts. The order of the CO conversion was Ru(Cl)/Al_2O_3 > Ru(A)/Al_2O_3 > Ru(N)/Al_2O_3. This order was also agreed with the order of CO conversion on Ru/Mn/Al_2O_3 catalysts in various Ru precursors. However, CO conversion decreased gradually with time on stream and deactivation rate was clearly observed over Ru/Al_2O_3 catalysts **(Fig. 5)**. The detail results are shown in **Table 3** for FT synthesis.

On the basis of hydrocarbon selectivity in **Table 3**, Ru(N)/Mn/Al_2O_3 showed higher selectivity of methane (CH_4) and lower selectivity of C_{5+} than those of other catalysts. It can be dependent on the particle size of catalysts. Particle size of Ru(N)/Mn/Al_2O_3 was about 6 nm, and this value was also lower than pore diameter

Table 2 Surface Concentrations and Binding Energies of Ru(Cl)/Mn/Al_2O_3 and Ru(Cl)/Al_2O_3 Catalysts by Using XPS Measurements

Catalysts[a)]	Surface atomic concentration [%]					Atomic ratio, Cl/Mn	Binding energy [eV]	
	Ru	Mn	Cl	O	Al		E_b[Ru^0][b)]	E_b[Mn][c)]
Ru/Mn/Al_2O_3	3.2	2.5	2.2	59.3	32.8	0.9	461.7	642.2
Ru/Al_2O_3	1.3	—	0.9	60.0	37.8	—	461.3	—

a) H_2 pretreatment at 473 K for 3 h inside the XPS pre-chamber.
b) Binding energy of Ru $3p_{3/2}$.
c) Binding energy of Mn $2p_{3/2}$.

such as 9 nm in **Table 1**. Although, oxide of manganese was observed in Ru(N)/Mn/Al_2O_3 according to the XRD results in **Fig. 2(i)**(e). These phenomenon can be controlled the yield of catalytic activity of Ru(N)/Mn/Al_2O_3 catalyst. In the case of Ru(A)/Mn/Al_2O_3, CO conversion was about 42% after the FT reaction at 40 h. Moreover, deactivation rate was much high during the reaction due to the low reducibility of catalyst, which confirmed by H_2 chemisorption and TPR. Furthermore, impurities on the surface were observed over Ru(A)/Mn/Al_2O_3 and Ru(N)/Mn/Al_2O_3 catalysts in TPR diagrams (**Figs. 1(d)** and **(e)**). On the other hand, selectivity of methane, middle distillate and olefin-paraffin ratio were observed in a great expectation for Ru(Cl)/Mn/Al_2O_3 catalyst, and space time yield and carbon chain growth probability were about 0.22 mol/g·h and 0.90, respectively. Furthermore, deactivation rate on Ru(Cl)/Mn/Al_2O_3 was negligible for FT synthesis. In an explanation, Ru(Cl)/Mn/Al_2O_3 catalyst showed almost similar middle size Ru particles and pore diameter such as 8 nm (**Table 1**), which can be performed to enhance catalytic activity for FT synthesis. These results are also in good agreement with previous reports[28)~30)]. For comparison, Ru(Cl)/Al_2O_3 showed lower CO conversion than Ru(Cl)/Mn/Al_2O_3, and deactivation rate was clearly observed with time on stream. It can be assumed that catalyst deactivation over Ru(Cl)/Al_2O_3 is related to the amount of residual chlorine ions as possible $RuCl_xO_y$ species leading to the decrease of active metallic Ru sites on the catalyst surface. Previous reports suggested that the residual chlorine ions are partitioned between the support and the metal, and that the chlorine on the surface could inhibit both CO and hydrogen chemisorption[12),13)]. According to the XPS results on Ru(Cl)/Mn/Al_2O_3 and Ru(Cl)/Al_2O_3 in **Table 2**, surface concentrations of Ru and Cl were increased on Ru(Cl)/Mn/Al_2O_3 than that on Ru(Cl)/Al_2O_3. Mn can influence to increase a removal of chlorine atom from ruthenium chloride by forming $MnCl_2$ species thus eliminating the deleterious effects of chlorine on CO and H_2 chemisorption. In this case, the concentration of metallic Ru, associated with catalytic performance in the FT reaction, increases. As a result, Ru/Mn/Al_2O_3 prepared with an aqueous solution of ruthenium chloride performed with high activity and high stability for FT synthesis. Therefore, FT activity in

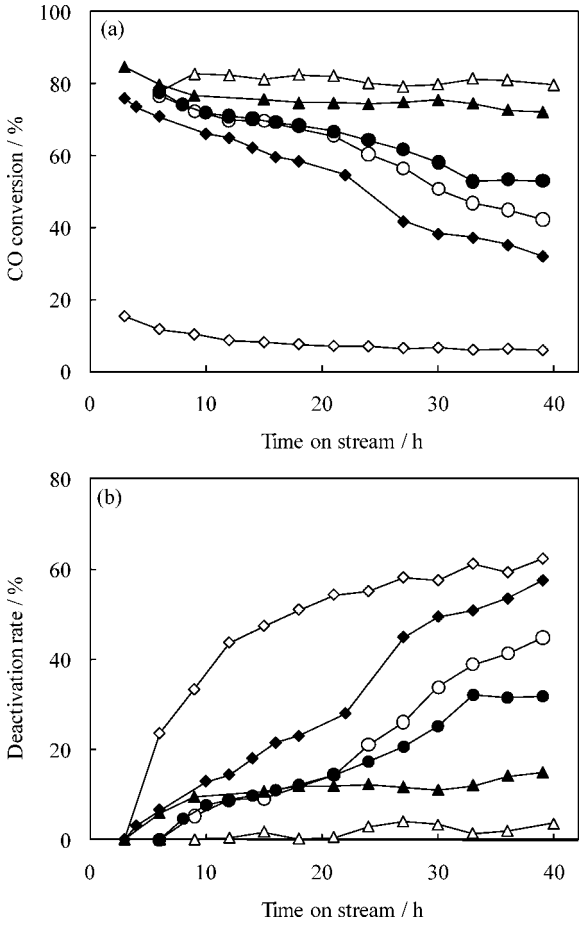

(△) Ru(Cl)/Mn/Al_2O_3, (○) Ru(A)/Mn/Al_2O_3, (◇) Ru(N)/Mn/Al_2O_3, (▲) Ru(Cl)/Al_2O_3, (●) Ru(A)/Al_2O_3, (◆) Ru(N)/Al_2O_3.
Reaction conditions: catalyst weight = 2.5 g, T = 493 K, P = 20 bar, H_2/CO = 2, GHSV = 1800 h^{-1}, H_2 reduction = 473 K.

Fig. 5 Reaction Time Dependence on (a) CO Conversion and (b) Deactivation Rate over Ru/Mn/Al_2O_3 and Ru/Al_2O_3 Catalysts for FT Synthesis

Table 3 Effect of Ru Precursors on Ru/Mn/Al_2O_3 and Ru/Al_2O_3 Catalysts for FT Synthesis

Catalyst	CO conv.[a)] [%]	CH_4 sel.[a)] [%]	C_{5+} sel.[a)] [%]	D[b)]	α[c)]
Ru(Cl)/Mn/Al_2O_3	80.0	2.3	89.2	3.6	0.90
Ru(A)/Mn/Al_2O_3	42.3	5.0	88.0	44.8	0.90
Ru(N)/Mn/Al_2O_3	5.8	51.6	37.9	62.3	0.86
Ru(Cl)/Al_2O_3	72.1	2.0	89.8	14.8	0.92
Ru(A)/Al_2O_3	53.0	3.4	89.1	31.9	0.91
Ru(N)/Al_2O_3	32.2	5.6	86.9	57.5	0.89

Reaction conditions: catalyst weight = 2.5 g, T = 493 K, P = 20 bar, H_2/CO = 2, GHSV = 1800 h^{-1}, TOS = 40 h, H_2 reduction = 473 K.
a) Results at 40 h TOS.
b) Deactivation rate: (CO conv. at 3 h − CO conv. at 40 h)/CO conv. at 3 h × 100.
c) Carbon chain growth probability.

$Ru/Mn/Al_2O_3$ catalysts is dependent on Ru precursors to prepare a catalyst for high performance.

4. Conclusions

(1) In the FT synthesis, Ru precursors are important to prepare $Ru/Mn/Al_2O_3$ catalyst. The aqueous solution of $RuCl_3$ is suitable as precursor to prepare Ru catalyst in the impregnation method for high performance of FT synthesis.
(2) $Ru(Cl)/Mn/Al_2O_3$ enhanced the catalytic activity and stability during FT reaction, where $Ru(A)/Mn/Al_2O_3$ and $Ru(N)/Mn/Al_2O_3$ showed low performance and deactivation rate was clearly observed.
(3) Catalyst characterization results indicate that particle size and pore diameter such as 8 nm can be controlled to enhance catalytic performance for FT synthesis. Over $Ru(Cl)/Mn/Al_2O_3$, lot of round-shaped particles were observed. Mn can increase the concentration of metallic Ru active species by removing chlorine atoms from ruthenium chloride, thus increasing catalytic activity while inhibiting catalyst deactivation.

Acknowledgment

TEM analysis was supported by the Research and Development Support Project of TEM, operated at AIST, Japan.

References

1) Rostrup-Nielsen, J. R., *Catal. Rev.*, **46**, 247 (2004).
2) Anderson, R. B., "The Fischer-Tropsch Synthesis," Academic Press, Orlando, FL. (1984).
3) Ernst, B., Libs, S., Chaumette, P., Kiennemann, A., *Appl. Catal. A: General*, **186**, 145 (1999).
4) Nurunnabi, M., Mukainakano, Y., Kado, S., Miyazawa, T., Okumura, K., Miyao, T., Naito, S., Suzuki, K., Fujimoto, K. I., Kunimori, K., Tomishige, K., *Appl. Catal. A: General*, **308**, 1 (2006).
5) Nurunnabi, M., Fujimoto, K. I., Suzuki, K., Li, B., Kado, S., Kunimori, K., Tomishige, K., *Catal. Commun.*, **7**, 73 (2006).
6) Mochizuki, T., Hara, T., Koizumi, N., Yamada, M., *Appl. Catal. A: General*, **317**, 97 (2007).
7) Dry, M. E., *Stud. Surf. Sci. Catal.*, **152**, 533 (2004).
8) Iglesia, E., Soled, S. L., Fiato, R. A., Via, G. H., *J. Catal.*, **143**, 345 (1993).
9) Huber, G. W., Guymon, C. G., Conrad, T. L., Stephenson, B. C., Bartholomew, C. H., *Stud. Surf. Sci. Catal.*, **139**, 423 (2001).
10) Hosseini, S. A., Taeb, A., Feyzi, F., *Catal. Commun.*, **6**, 233 (2005).
11) Reinikainen, M., Niemela, M. K., Kakuta, N., Suhonen, S., *Appl. Catal. A: General*, **174**, 61 (1998).
12) Ragaini, V., Carli, R., Bianchi, C. L., Lorenzetti, D., Vergani, G., *Appl. Catal. A: General*, **139**, 17 (1996).
13) Narita, T., Miura, H., Ohira, M., Hondou, H., Sugiyama, K., Matsuda, T., *Appl. Catal.*, **32**, 185 (1987).
14) Morales, F., de Groot, F. M. F., Gijzeman, O. L. J., Mens, A., Stephan, O., Weckhuysen, B. M., *J. Catal.*, **230**, 301 (2005).
15) Bezemer, G. L., Radstake, P. B., Falke, U., Oosterbeek, H., Kuipers, H. P. C. E., van Dillen, A. J., de Jong, K. P., *J. Catal.*, **237**, 152 (2006).
16) Nurunnabi, M., Murata, K., Okabe, K., Inaba, M., Takahara, I., *Appl. Catal. A: General*, **340**, 203 (2008).
17) Nurunnabi, M., Murata, K., Okabe, K., Inaba, M., Takahara, I., *Catal. Commun.*, **8**, 1531 (2007).
18) Nurunnabi, M., Murata, K., Okabe, K., Inaba, M., Takahara, I., *J. Jpn. Petrol. Inst.*, **51**, (4), 252 (2008).
19) Betancourt, P., Rives, A., Hubaut, R., Scott, C. E., Goldwasser, J., *Appl. Catal. A: General*, **170**, 307 (1998).
20) Mazzieri, V., Coloma-Pascual, F., Arcoya, A., Argentiere, P. C. L., Figoli, N. S., *Appl. Surf. Sci.*, **210**, 222 (2003).
21) Koopman, P. G. J., Kieboom, A. P. G., van Bekkum, H., *J. Catal.*, **69**, 172 (1981).
22) Eliche-Quesada, D., Merida-Robles, J. M., Rodriguez-Castellon, E., Jimenez-Lopez, A., *Appl. Catal. A: General*, **279**, 209 (2005).
23) ICDD, 88-0323.
24) ICDD, 06-0663.
25) ICDD, 78-0390.
26) Nurunnabi, M., Murata, K., Okabe, K., Inaba, M., Takahara, I., "Advances in Fischer-Tropsch Synthesis, Catalysts and Catalysis," eds. by Davis, B. H., Occelli, M. L., Vol. 128, CRC Press, New York (2009), Chap. 5, p. 83-94.
27) Kapteijn, F., van Langeveld, A. D., Moulijn, J. A., Andreini, A., Vuurman, M. A., Turekm, A. M., Jehng, J. M., Wachs, I. E., *J. Catal.*, **150**, 94 (1994).
28) Shinoda, M., Zhang, Y., Yoneyama, Y., Hasegawa, K., Tsubaki, N., *Fuel Process. Technol.*, **86**, 73 (2004).
29) Khodakov, A. Y., Constant, A. G., Bechara, R., Zholobenko, V. L., *J. Catal.*, **206**, 230 (2002).
30) Bezemer, G. L., Bitter, J. H., Kuipers, H. P. C. E., Oosterbeek, H., Holewijn, J. E., Xu, X., Kapteijn, F., van Dillen, A. J., de Jong, K. P., *J. Am. Chem. Soc.*, **128**, 3956 (2006).

要　　旨

Fischer-Tropsch 合成のための $Ru/Mn/Al_2O_3$ および Ru/Al_2O_3 触媒におけるルテニウム前駆体依存性

Mohammad NURUNNABI，村田　和久，岡部　清美，花岡　寿明，宮澤　朋久，坂西　欣也

（独）産業技術総合研究所 バイオマス研究センター，737-0197 広島県呉市広末広2-2-2産総研中国センター

種々のルテニウム前駆体より含浸法で調製した $Ru/Mn/Al_2O_3$ および Ru/Al_2O_3 触媒を用いて流通式撹拌反応装置にて Fischer-Tropsch（FT）反応試験を行い，H_2 吸着量測定，TPR，XRD，TEM および XPS の各種キャラクタリゼーションを行った。$Ru/Mn/Al_2O_3$ については，塩化ルテニウムより調製した $Ru(Cl)/Mn/Al_2O_3$ がアセチルアセトナトルテニウムおよびニトロシル硝酸ルテニウムより調製した $Ru(A)/Mn/Al_2O_3$，$Ru(N)/Mn/Al_2O_3$ よりも高い活性と安定性を示した。CO 転化率は $Ru(Cl)/Mn/Al_2O_3 \gg Ru(A)/Mn/Al_2O_3 > Ru(N)/Mn/Al_2O_3$ の順であり，この序列は同様に前駆体を変えた Ru/Al_2O_3 の場合の CO 転化率の序列と一致した。キャラクタリゼーションの結果，ルテニウム粒子径および担体の細孔径が 8 nm サイズであることが高い FT 活性に寄与していることが示唆される。また，$Ru(Cl)/Mn/Al_2O_3$ と $Ru(Cl)/Al_2O_3$ 触媒を比較すると，$Ru(Cl)/Mn/Al_2O_3$ が触媒劣化への高い耐性を示したのに対して，$Ru(Cl)/Al_2O_3$ 上では低い活性と急速な活性劣化が顕著に見られた。この結果から，塩化ルテニウムより塩素原子を奪う形で塩化マンガンが生じることにより，触媒表面上の金属ルテニウム活性種が増加し，触媒活性劣化が抑制されると考えられる。

……